ACS APPLIED MATERIALS & INTERFACES

Research Article

www.acsami.org

Uniformly Wetting Deposition of Co Atoms on MoS_2 Monolayer: A Promising Two-Dimensional Robust Half-Metallic Ferromagnet

Qian Chen,[†,⊥] Yixin Ouyang,[†,⊥] Shijun Yuan,[†] Runze Li,[‡] and Jinlan Wang*[,†,§]

[†]Department of Physics, [‡]Chien-Shiung Wu College, and [§]Key Laboratory of MEMS of Ministry of Education, Southeast University, Nanjing 211189, China

ABSTRACT: Synthesis of two-dimensional (2D) metal chalcogenide based half-metallic nanosheets is in high demand for modern electronics and spintronics applications. Herein, we predict from first-principles calculations that the 2D heterostructure Co/MoS_2, consisting of a monolayer of Co atoms deposited on a single MoS_2 sheet, possesses robust ferromagnetic and half-metallic features and exhibits 100% spin-filter efficiency within a broad bias range. Its ferromagnetic and half-metallic nature persists even when overlaid with a graphene sheet. Because of the relatively strong surface binding energy and low clustering ratio of Co atoms on the MoS_2 surface, we predict that the heterostructure is synthesizable via wetting deposition of Co on MoS_2 by electron-beam evaporation technique. Our work strongly suggests Co/MoS_2 as a compelling and feasible candidate for highly effective information and high-density memory devices.

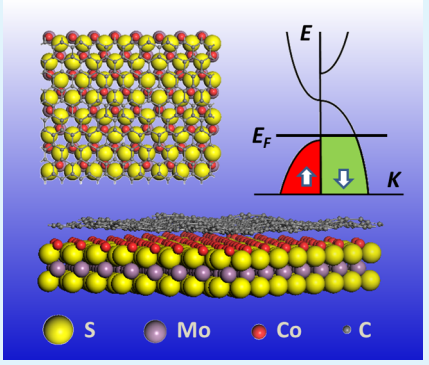

KEYWORDS: *metal chalcogenide, surface, spintronics, and density functional theory*

INTRODUCTION

Layered two-dimensional (2D) materials, such as graphene, hexagonal boron nitride (*h*-BN), and molybdenum disulfide (MoS_2) monolayer, have attracted great interest in recent years,[1−7] owing to their unusual mechanical, electronic, optical, and thermal properties arising from quantum confinement effects associated with atomically thin layers. Unlike semimetallic graphene and highly insulating *h*-BN, monolayer MoS_2 (ML-MoS_2) is an intrinsic semiconductor with a direct band gap of ∼1.8 eV that has demonstrated high on/off ratios (>1 × 10^8).[8,9] MoS_2 based semiconductor devices such as field-effect transistors,[5] digital circuits[10] have been successfully fabricated. Very recently, a long spin lifetime of more than 1 ns has been detected in polarization-resolved photoluminescence measurements,[11] demonstrating that the spin lifetimes in MoS_2 have outpaced that in graphene. This is because the spin−orbit coupling and absence of inversion symmetry in MoS_2 suppress spin relaxation and hence, enhances the spin lifetimes.[12] These findings have stimulated our enthusiasm to study novel 2D monolayer MoS_2 based semiconductor spintronic devices.

Transition metals (TMs), such as Mn, Fe, Co, dopants in monolayer MoS_2 have been predicted to result in 2D diluted magnetic semiconductors.[13−15] However, dilute doping is difficult in experiments,[16] thus it is important to find alternative ways to introduce magnetism into ML-MoS_2. Via the magnetic proximity effect,[17] spin injection from a high spin-polarized ferromagnetic electrode seems promising.[18] However, scientists have yet to establish a method to fabricate ferromagnet/MoS_2 interfaces for efficient spin injections, a result of the large conductivity mismatches and volatile tunnel barriers at the interfaces.[19,20] It is well-known that the most efficient method for spin injection is to introduce half-metallic ferromagnets, which can create fully spin-polarized carriers.[21,22] It is of great importance and interest to synthesize 2D MoS_2-based ferromagnetic or even half-metallic homoepitaxial structures to achieve efficient spin injections. In this work, we predict a new 2D half-metallic Co/MoS_2 heterojunction with robust ferromagnetic ground spin state and 100% spin current polarization within the framework of density functional theory (DFT). Relatively high Co surface binding energies and high diffusion barriers suggest experimental synthesis via a wetting growth mechanism of Co atoms on ML-MoS_2 is highly feasible.

COMPUTATIONAL METHODS

The spin-polarized DFT calculations were carried out within a general gradient approximation parametrized by Perdew, Burke, and Ernzerhof,[23] as implemented in Vienna ab initio simulation package.[24,25] Projected augmented wave method[26] was employed to describe the electron−ion potential, and a kinetic energy cutoff of 400 eV was used for the plane wave expansion. We adopted a 5 × 5 × 1 supercell and a 5 × 5 × 1 k-point grid for the Brillouin zone. The vacuum spaces in all supercells were more than 10 Å above the MoS_2 plane to avoid any artificial interaction. The energy cutoff and k-point mesh have been tested to make the energy difference less than 10 meV. The calculated lattice constant and direct band gap of monolayer MoS_2 are 3.18 Å and 1.67 eV, respectively, in fair agreement with earlier results.[27,28]

We performed the climbing-image nudged elastic band (cNEB) method[29] to locate the minimum energy paths and the transition states of Co atoms on MoS_2 sheet. The effect of van der Waals (vdW) interactions was included for weak interaction cases and described

Received: June 29, 2014
Accepted: September 3, 2014
Published: September 4, 2014

using the semiempirical correction scheme of Grimme, DFT-D2.[30] Charge and spin transport properties were done with the TRANSIESTA code,[31] and the density matrix of the scattering region was calculated self-consistently in the presence of an external bias by means of the nonequilibrium Green's function method.[32]

RESULTS AND DISCUSSION

We first consider single Co atom adsorption on MoS_2. Different adsorption positions, such as Mo-top, S-top and hollow site, should be considered. In agreement with ref 33, our calculations show that the Mo-top site, labeled as 1 in Figure 1a, is the most stable one. And the hollow and S-top site (labeled as 2 and t1 in Figure 1a) are 0.28 and 1.65 eV higher in energy, respectively. As shown in Figure 1a, the S-top site is a transition state based on the cNEB calculations, and with any small perturbation, the Co on S-top will slip to the neighboring Mo-top or hollow site without any barrier, whereas if the Co atom is at the Mo-top site, it needs to climb a barrier of 0.79 eV at least to the nearest local minimum (the hollow site). This barrier is much higher than 0.40 eV of Co/graphene and 0.13 eV of Co/*h*-BN,[34,35] and the diffusion path involves a transition state at the bridge between two S atoms (t2-site). In addition, the desorption of the Co atom from MoS_2 needs to gain a kinetic energy of more than 3.10 eV, and the desorbed state (labeled as 3) is also presented in Figure 1a. This energy is again significantly higher than 1.60 eV of Co/graphene and 1.03 eV of Co/*h*-BN.[34,35] As graphene or *h*-BN has a "flat" π electron cloud because of the sp^2 network, TMs have relatively weak binding with graphene and can diffuse with low barrier. In contrast, MoS_2 nanosheet has sandwich S−Mo−S structure and the coexistence of Mo-4d and S-3p orbitals at the band edges.[36] This makes a periodically uneven surface both in real geometry and potential energy space, and results in the stronger bonding with Co atoms. The Co atom adsorbed MoS_2 possesses a net magnetic moment of 0.93 μ_B. The spin density, as depicted in the inset of Figure 1a, shows that the magnetic moment mainly locates on the Co atom.

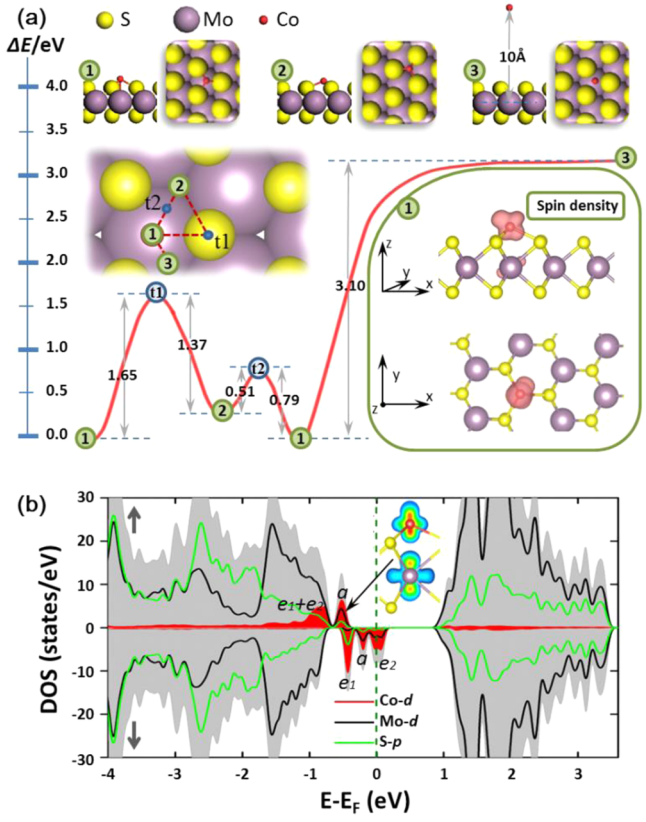

Figure 1. (a) Diffusion path of a single Co atom adsorbed on monolayer MoS_2. The local minima and transition states are labeled as 1, 2 and t1, t2, respectively, and the desorbed state is labeled as 3. The corresponding structures, including top and side views, are presented in the upper. The yellow, purple and red balls refer to the S, Mo, and Co atoms, respectively. The spin density of the configuration 1 is in the lower right corner, with an iso-surface of 0.005 $e/Å^3$. (b) Spin-resolved PDOS of configuration 1. The gray region is the total DOS of the supercell and the dashed vertical line refers to the Fermi level. The up and down arrows indicate the spin-up and spin-down channels, respectively. The inset is the charge density profile of "*a*" states at the arrowhead.

To further understand the magnetic splitting effect and the origin of high binding energy, the evolution of spin-resolved projected density of states (PDOS) of Co/MoS_2 is displayed in Figure 1b. The states near the Fermi level (E_F) are dominated by the Co 3d orbitals and have a large exchange splitting. As Co atom adsorbing at the Mo-top site obtains a C_{3v} symmetry, the five 3d states further split into three groups in each spin channel: e_1, e_2, and *a*. The Co e_1 (d_{xy}, $d_{x^2-y^2}$) orbitals and e_2 (d_{xz}, d_{yz}) orbitals that facing MoS_2 significantly hybrid with S 3p orbitals and present at relatively low energy levels in the spin-up channel, whereas those Co orbitals on the side back to MoS_2 have weak overlap with S 3p, corresponding to those higher energy and more localized peaks in the spin-down channel. The inset of Figure 1b is the charge density of the *a* states, from which we can see a $\sigma-\sigma$ bond between the Co d_{z^2} and the underlying Mo d_{z^2} orbitals. This makes the binding energy of Co at Mo-top larger than that at the hollow site by about 0.28 eV (see Figure 1a).

We then explore the energetic and kinetic properties of two Co atoms on MoS_2 surface. Figure 2a shows an energy pathway of two Co adatoms getting close, from which we can see the lowest energy configuration corresponding to the neighboring two Mo-top sites, labeled with "3". This configuration has lower energy than that of the separated ones (configuration 1) with 0.37 eV, and with a significant barrier of 1.11 eV. This suggests that the Co adatoms tend to have certain interactions to further stabilize themselves. Additionally, the interactions can also be reflected in the magnetic coupling, which results in an energetically favorable FM coupling state with 166 meV lower than that of the antiferromagnetic (AFM) state (see the inset of Figure 2a). The energy difference of FM and AFM states ($E_{\uparrow\uparrow} - E_{\uparrow\downarrow}$) is only −80 meV when two Co atoms are separated as in configuration 1. Nevertheless, as the two Co atoms get further closer and form a Co−Co dimer on MoS_2 (see configuration 4 in Figure 2a), the total energy goes up by 1.02 eV and with a barrier of 1.88 eV. This suggests that such interadsorbate interaction is still weaker than the adsorbate−substrate interaction and heralds the uniformly wetting growth of Co atoms on MoS_2.[37,38]

To further confirm the uniformly wetting growth pattern of Co atoms on MoS_2 and the preferred FM coupling, we add another Co atom on the substrate. As shown in Figure 2b, the triangular arrangement of the Co atoms locating on Mo-top site (configuration 6) is most stable, and the barrier to break the configuration is about 0.89 eV. When the third Co atom goes away or gets close, the energies both go up more than 0.40 eV. In particular, the Co_3 cluster on MoS_2 is a transition state on

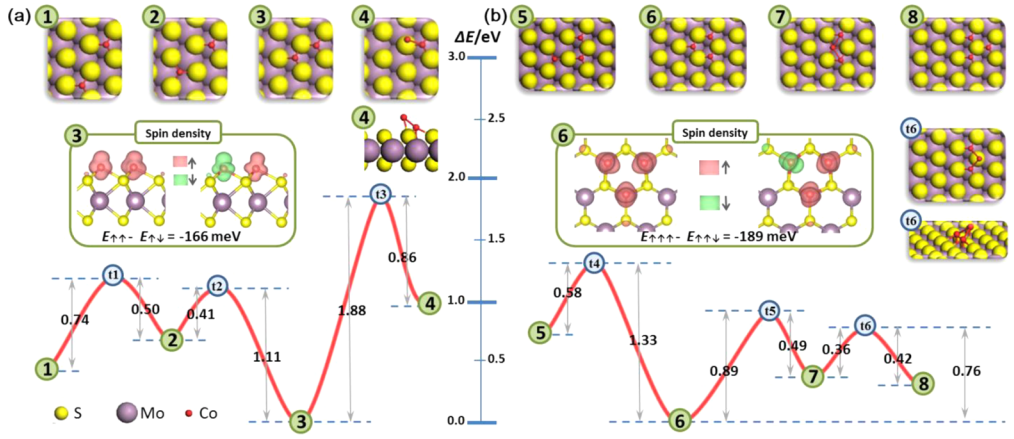

Figure 2. Minimum diffusion path of (a) two Co atoms and (b) three Co atoms adsorbed on ML-MoS_2. The local minima and transition states are labeled as 1, 2, ... and t1, t2, ..., respectively. The corresponding structures are presented in the upper part. The insets are the spin density of the configuration 3 and 6, with an iso-surface of 0.005 e/ Å^3.

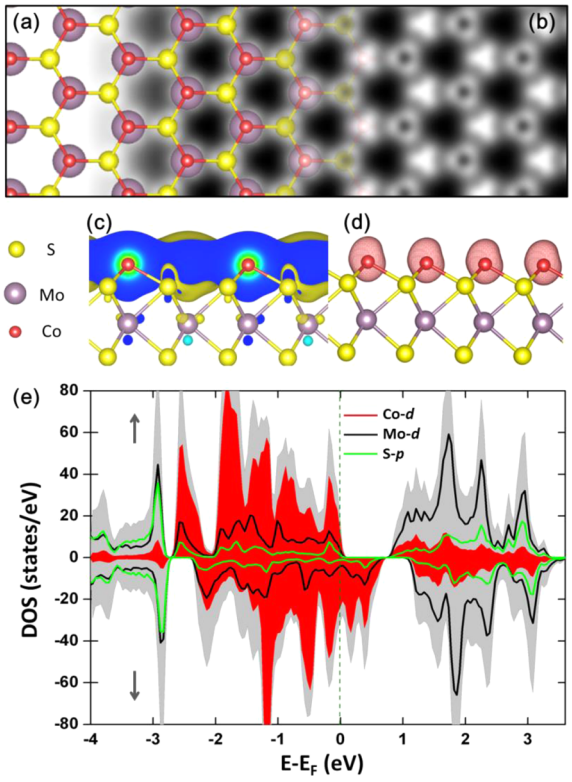

Figure 3. (a) Top view of the relaxed atomic structure of monolayer Co atoms on MoS_2. (b) DFT simulated STM image for bias of −1.0 V. Charge density difference profile (c) and spin density (d) of the structure, the iso-surface is 0.005 e/Å^3. (e) Spin-resolved PDOS of ML-Co/MoS_2. The gray region is the total DOS of the supercell and the dashed vertical line refers to the Fermi level. The up and down arrows indicate the spin-up and spin-down channels, respectively.

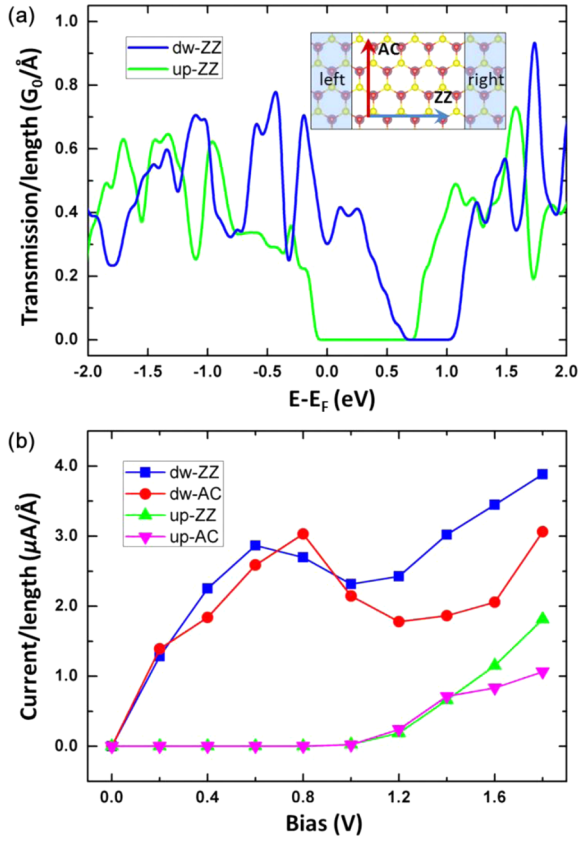

Figure 4. (a) Spin-dependent transmission spectrum of ML-Co/MoS_2 in zigzag direction with zero bias. The light green line is for the spin-up transmittance channel and the dark blue line is for the spin-down channel. The inset is the schematic illustration of the calculation model. (b) Spin-dependent I−V_{bias} curves in both zigzag and armchair directions, respectively.

the energy pathway (configuration t6) with 0.76 eV higher than the ground state. This suggests that the relative strength of interadsorbate and adsorbate−substrate interactions is just right to form uniform film morphology of Co on MoS_2 and stable FM coupling state. We expect this heterostructure can be achieved via wetting deposition of Co on MoS_2 from the electron-beam evaporator at suitable temperature.[39] The inset of Figure 2b shows the spin density of the FM (↑↑↑) and ferrimagnetic (↑↑↓) coupling states, and the FM coupling state with 189 meV lower than that of the ferrimagnetic state in energy, that is, $E_{\uparrow\uparrow\uparrow} - E_{\uparrow\uparrow\downarrow} = -189$ meV.

Next, we come to the fully covered MoS_2 with Co atoms adsorbing on the Mo-top site (ML-Co/MoS_2). Figure 3 presents the optimized atomic structure and the corresponding simulated image from scanning tunneling microscopy (STM) for a bias of −1.0 V. The calculated lattice constant is 3.23 Å with C_{3v} symmetry, and the Co adatoms can be clearly seen in

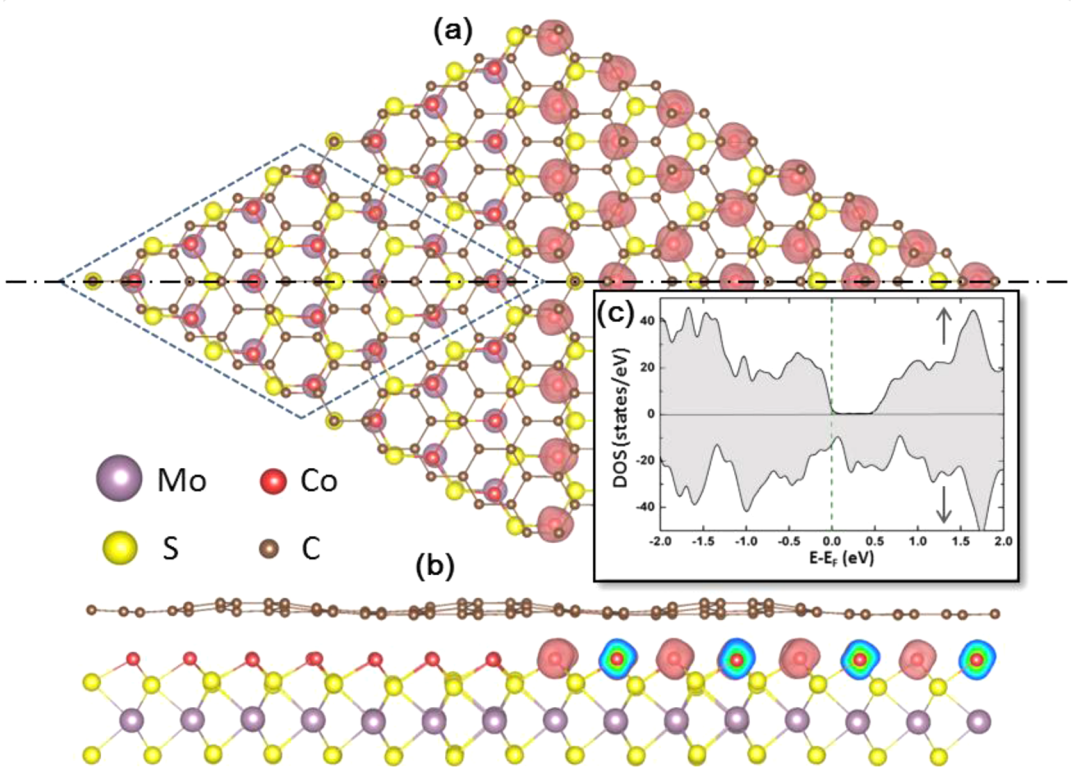

Figure 5. (a) Top view of the relaxed atomic structure for graphene covered ML-Co/MoS_2 (Gr/Co/MoS_2). The spin density is presented in the right panel with an iso-surface of 0.01 $e/Å^3$. The dashed rhombus represents the supercell. (b) Side view across the dash and dot line. (c) Partial DOS of ML-Co/MoS_2 in Gr/Co/MoS_2.

the STM image. The E_b here is 3.95 eV/Co, larger than those of single, double and trifoliate adsorption configurations aforementioned (3.95 vs 3.10, 3.49, 3.68 eV/Co). As clearly shown in Figure 3c that the local charge density around the Co atoms is presented, besides evident bonding between Co−S atoms, a significant downward bulge of the charge density witnesses the strong interaction between Co and underneath Mo atom with the d_{z^2} orbitals. Additionally, there is weak overlap of neighboring Co orbitals, which also contributes to the high E_b of ML-Co/MoS_2. This interaction also results in the FM coupling of Co atoms with a net magnetic moment of about 0.90 μ_B per Co atom, which mainly originates from the d orbitals of Co atoms (see the spin density presented in Figure 3d).

To calculate Co−Co exchange interaction J and Curie temperature T_C, we used effective Heisenberg Hamiltonian $H = -J \sum \mathbf{S}_i \cdot \mathbf{S}_j$ and mean field approximation (MFA) method here.[40] The Curie temperature is given by $T_C = zJ/k_B$, where z is the number of nearest neighbor Co atoms and k_B is the Boltzmann constant. By comparing the total energy (per formula unit) of FM and AFM state, the calculated exchange parameters of the nearest two Co sites is 6.99 meV. The estimated magnetic ordering temperature is about 486 K, which is substantially higher than room temperature. Note that the MFA neglects the effect of fluctuation of the spins from their average values, which tends to decrease the magnetic ordering temperature. Therefore, the MFA often gives an overestimation of the actual ordering temperature. However, it still can provide a clue and theoretical understanding for further experimental study.

Figure 3e displays the PDOS of ML-Co/MoS_2. There are heavy overlaps among Co-d, Mo-d, and S-p orbitals, and the band edge structures change remarkably in comparison with those of pristine MoS_2. This suggests the strong bonding between monolayer Co and MoS_2 which eventually results in the formation of the stable 2D heterostructure. Large spin-splitting near the E_F is observed corresponding to the large net magnetism (see Figure 3d)). More interestingly, the DOS shows conductance for the spin-down orientation electrons and a semiconducting band gap in the spin-up channel, known as half-metallic property.[21] Thus, it is expected to provide 100% spin-polarized current and promises fantastic potential use in spintronics.

We further explore the transport properties of monolayer Co on MoS_2. The spin-dependent zero-bias transmission spectrum along the zigzag direction is presented in Figure 4a. Within the energy range $0 < E - E_F < 0.7$ eV, the spin-down channel is opened up while the spin-up channel is completely suppressed. As a consequence, the spin-down current shows metallic behavior and the spin-up current is completely blocked (see Figure 4b), demonstrating a perfect spin filter efficiency. Furthermore, the spin-dependent $I-V_{bias}$ curves exhibit 100% spin-filter efficiency with a bias ranging from 0 to more than 1 V in both zigzag and armchair directions. Such wide bias-range of spin-polarized current and regardless of direction makes this 2D material very attractive in practical applications in spintronic devices.

To resist the complex environmental influence on the performance of devices, protective coating is a commonly used way in manufacturing process.[41] Whether key properties could survive after covering with protective layers is thereby of great

importance. Because of unique atomic layer structure,[42] highly impermeability to gases,[43] and itself robustness against oxidation,[44] graphene is a promising new coating material that could be effective for anticorrosion. Here, taking graphene as the covering material, we further investigate the graphene coated monolayer Co on MoS_2 (namely, Gr/Co/MoS_2). A commensurability condition between graphene and ML-Co/MoS_2 was imposed, where a 5 × 5 periodicity of the graphene and 4 × 4 periodicity of ML-Co/MoS_2 were employed.[45] The optimized structure is shown in panels a and b in Figure 5, the lattice parameter is 12.5 Å, which comprises of +1.9% and −3.1% lattice mismatch for isolated graphene and ML-Co/MoS_2, respectively. The lattice mismatch results in undulations of graphene, known as Moirè patterns. The distances between graphene and ML-Co/MoS_2 vary from 2.20 to 2.50 Å, and both are longer than that of Co atoms adsorbed on graphene (about 1.50 Å).[46] The binding energy, calculated by subtracting energy of free-standing graphene and ML-Co/MoS_2 from that of Gr/Co/MoS_2, is 0.30 eV per Co atom, much smaller than isolate Co atom binding with graphene (1.60 eV)[34] or with MoS_2 (3.10 eV). Such relatively long distance and small binding energy suggest that the graphene bonds to ML-Co/MoS_2 via weak interactions like vdW interaction and electrostatic interaction, rather than orbital hybridization. The Gr/Co/MoS_2 heterojunction structure maintains a FM state with ∼1.0 μ_B located on each Co atom, as shown in the right panel of Figure 5a and b. Moreover, partial DOS of Co/MoS_2 in Gr/Co/MoS_2 shows a half-metallic property as well (see in Figure 5c). The robust FM and half-metallic properties may make this atomic thin 2D magnetic semiconductor serve as building block for spintronic related applications.

CONCLUSION

In summary, we have simulated uniformly wetting growth of single layer Co atoms on monolayer MoS_2. Strong surface binding energy and low clustering tendency of Co atoms on the MoS_2 surface are keys for successfully obtaining a uniform layer. Actually, Co−Mo interaction plays a crucial role in pinning the atomic Co. More interestingly, the surface Co atoms tend to form highly stable ferromagnetic states and exhibit a 100% current polarization (half-metal) in the newly formed 2D ML-Co/MoS_2 heterojunction structure, which can sustain the ferromagnetic state and half-metallic property when overlaid with a graphene sheet. Very recently, it is also reported that monolayers of iron[47] and hafnium[39] have been successfully in experiments. Our theoretical calculation provides justifications for follow-up experimental synthesis of Co/MoS_2 and may be used to anticipate the synthesis of other novel 2D magnetic structures that are yet to be explored.

AUTHOR INFORMATION

Corresponding Author

*E-mail: jlwang@seu.edu.cn.

Author Contributions

⊥These authors contributed equally to this work.

Notes

The authors declare no competing financial interest.

ACKNOWLEDGMENTS

This work, carried out by the SEU, is supported by the NBRP (2010CB923401, 2011CB302004), NSFC (21173040, 21373045, 11247285, 11404056), the NSF of Jiangsu (BK2012322, BK20130016), SRFDP (20130092110029, 20130092120042) of China, and SEU. The computational resources were provided by SEU and National Supercomputing Center in Tianjin.

REFERENCES

(1) Novoselov, K. S.; Geim, A. K.; Morozov, S. V.; Jiang, D.; Zhang, Y.; Dubonos, S. V.; Grigorieva, I. V.; Firsov, A. A. Electric Field Effect in Atomically Thin Carbon Films. *Science* **2004**, *306*, 666−669.

(2) Yakobson, B. I.; Ding, F. Observational Geology of Graphene, at the Nanoscale. *ACS Nano* **2011**, *5*, 1569−1574.

(3) Zeng, H.; Zhi, C.; Zhang, Z.; Wei, X.; Wang, X.; Guo, W.; Bando, Y.; Golberg, D. "White Graphenes": Boron Nitride Nanoribbons via Boron Nitride Nanotube Unwrapping. *Nano Lett.* **2010**, *10*, 5049−5055.

(4) Zhang, Z. H.; Zeng, X. C.; Guo, W. L. Fluorinating Hexagonal Boron Nitride into Diamond-Like Nanofilms with Tunable Band Gap and Ferromagnetism. *J. Am. Chem. Soc.* **2011**, *133*, 14831−14838.

(5) Radisavljevic, B.; Radenovic, A.; Brivio, J.; Giacometti, V.; Kis, A. Single-layer MoS_2 transistors. *Nat. Nanotechnol.* **2011**, *6*, 147−150.

(6) Coleman, J. N.; Lotya, M.; O'Neill, A.; Bergin, S. D.; King, P. J.; Khan, U.; Young, K.; Gaucher, A.; De, S.; Smith, R. J.; Shvets, I. V.; Arora, S. K.; Stanton, G.; Kim, H. Y.; Lee, K.; Kim, G. T.; Duesberg, G. S.; Hallam, T.; Boland, J. J.; Wang, J. J.; Donegan, J. F.; Grunlan, J. C.; Moriarty, G.; Shmeliov, A.; Nicholls, R. J.; Perkins, J. M.; Grieveson, E. M.; Theuwissen, K.; McComb, D. W.; Nellist, P. D.; Nicolosi, V. Two-Dimensional Nanosheets Produced by Liquid Exfoliation of Layered Materials. *Science* **2011**, *331*, 568−571.

(7) Qiu, H.; Xu, T.; Wang, Z.; Ren, W.; Nan, H.; Ni, Z.; Chen, Q.; Yuan, S.; Miao, F.; Song, F.; Long, G.; Shi, Y.; Sun, L.; Wang, J.; Wang, X. Hopping Transport Through Defect-induced Localized States in Molybdenum Disulphide. *Nat. Commun.* **2013**, *4*, 2642−2647.

(8) Wang, Q. H.; Kalantar-Zadeh, K.; Kis, A.; Coleman, J. N.; Strano, M. S. Electronics and Optoelectronics of Two-dimensional Transition Metal Dichalcogenides. *Nat. Nanotechnol.* **2012**, *7*, 699−712.

(9) Mak, K. F.; Lee, C.; Hone, J.; Shan, J.; Heinz, T. F. Atomically Thin MoS_2: A New Direct-Gap Semiconductor. *Phys. Rev. Lett.* **2010**, *105*, 136805.

(10) Radisavljevic, B.; Whitwick, M. B.; Kis, A. Integrated Circuits and Logic Operations Based on Single-Layer MoS_2. *ACS Nano* **2011**, *5*, 9934−9938.

(11) Mak, K. F.; He, K. L.; Shan, J.; Heinz, T. F. Control of Valley Polarization in Monolayer MoS_2 by Optical Helicity. *Nat. Nanotechnol.* **2012**, *7*, 494−498.

(12) Xiao, D.; Liu, G. B.; Feng, W. X.; Xu, X. D.; Yao, W. Coupled Spin and Valley Physics in Monolayers of MoS_2 and Other Group-VI Dichalcogenides. *Phys. Rev. Lett.* **2012**, *108*, 196802.

(13) Mishra, R.; Zhou, W.; Pennycook, S. J.; Pantelides, S. T.; Idrobo, J.-C. Long-range Ferromagnetic Ordering in Manganese-doped Two-dimensional Dichalcogenides. *Phys. Rev. B* **2013**, *88*, 144409.

(14) Ramasubramaniam, A.; Naveh, D. Mn-doped Monolayer MoS_2: An Atomically Thin Dilute Magnetic Semiconductor. *Phys. Rev. B* **2013**, *87*, 195201.

(15) Cheng, Y. C.; Zhu, Z. Y.; Mi, W. B.; Guo, Z. B.; Schwingenschlogl, U. Prediction of Two-dimensional Diluted Magnetic Semiconductors: Doped Monolayer MoS_2 Systems. *Phys. Rev. B* **2013**, *87*, 100401.

(16) Komsa, H.-P.; Kotakoski, J.; Kurasch, S.; Lehtinen, O.; Kaiser, U.; Krasheninnikov, A. V. Two-Dimensional Transition Metal Dichalcogenides under Electron Irradiation: Defect Production and Doping. *Phys. Rev. Lett.* **2012**, *109*, 035503.

(17) Manna, P. K.; Yusuf, S. M. Two Interface Effects: Exchange Bias and Magnetic Proximity. *Phys. Rep.* **2014**, *535*, 61−99.

(18) Dash, S. P.; Sharma, S.; Patel, R. S.; de Jong, M. P.; Jansen, R. Electrical Creation of Spin Polarization in Silicon at Room Temperature. *Nature* **2009**, *462*, 491−494.

(19) Schmidt, G.; Ferrand, D.; Molenkamp, L. W.; Filip, A. T.; van Wees, B. J. Fundamental Obstacle for Electrical Spin Injection from a

Ferromagnetic Metal into a Diffusive Semiconductor. *Phys. Rev. B* **2000**, *62*, R4790−4793.
(20) Chen, J. R.; Odenthal, P. M.; Swartz, A. G.; Floyd, G. C.; Wen, H.; Luo, K. Y.; Kawakami, R. K. Control of Schottky Barriers in Single Layer MoS2 Transistors with Ferromagnetic Contacts. *Nano Lett.* **2013**, *13*, 3106−3110.
(21) Katsnelson, M. I.; Irkhin, V. Y.; Chioncel, L.; Lichtenstein, A. I.; de Groot, R. A. Half-metallic Ferromagnets: From Band Structure to Many-body Effects. *Rev. Mod. Phys.* **2008**, *80*, 315−378.
(22) Shen, L.; Yang, S. W.; Ng, M. F.; Ligatchev, V.; Zhou, L. P.; Feng, Y. P. Charge-transfer-based Mechanism for Half-metallicity and Ferromagnetism in One-dimensional Organometallic Sandwich Molecular Wires. *J. Am. Chem. Soc.* **2008**, *130*, 13956−13960.
(23) Perdew, J. P.; Burke, K.; Ernzerhof, M. Generalized Gradient Approximation Made Simple. *Phys. Rev. Lett.* **1996**, *77*, 3865−3868.
(24) Kresse, G.; Hafner, J. *Ab initio* Molecular Dynamics for Liquid Metals. *Phys. Rev. B* **1993**, *47*, 558−561.
(25) Kresse, G.; Furthmuller, J. Efficient Iterative Schemes for *ab initio* Total-energy Calculations Using a Plane-wave Basis Set. *Phys. Rev. B* **1996**, *54*, 11169−11186.
(26) Blöhl, P. E. Projector Augmented-wave Method. *Phys. Rev. B* **1994**, *50*, 17953−17979.
(27) Li, Y.; Zhou, Z.; Zhang, S.; Chen, Z. MoS_2 Nanoribbons: High Stability and Unusual Electronic and Magnetic Properties. *J. Am. Chem. Soc.* **2008**, *130*, 16739−16744.
(28) Johari, P.; Shenoy, V. B. Tuning the Electronic Properties of Semiconducting Transition Metal Dichalcogenides by Applying Mechanical Strains. *ACS Nano* **2012**, *6*, 5449−5456.
(29) Henkelman, G.; Uberuaga, B. P.; Jonsson, H. A Climbing Image Nudged Elastic Band Method for Finding Saddle Points and Minimum Energy Paths. *J. Chem. Phys.* **2000**, *113*, 9901−9904.
(30) Grimme, S. S. GGA-type Density Functional Constructed with a Long-range Dispersion Correction. *J. Comput. Chem.* **2006**, *27*, 1787−1799.
(31) Brandbyge, M.; Mozos, J. L.; Ordejon, P.; Taylor, J.; Stokbro, K. Density-functional Method for Nonequilibrium Electron Transport. *Phys. Rev. B* **2002**, *65*, 165401.
(32) Meir, Y.; Wingreen, N. S. Landauer Formula for the Current Through an Interacting Electron Region. *Phys. Rev. Lett.* **1992**, *68*, 2512−2515.
(33) Ataca, C.; Ciraci, S. Functionalization of Single-Layer MoS_2 Honeycomb Structures. *J. Phys. Chem. C* **2011**, *115*, 13303−13311.
(34) Yazyev, O. V.; Pasquarello, A. Metal Adatoms on Graphene and Hexagonal Boron Nitride: Towards Rational Design of Self-assembly Templates. *Phys. Rev. B* **2010**, *82*, 045407.
(35) Auwarter, W.; Muntwiler, M.; Greber, T.; Osterwalder, J. Co on h-BN/Ni(111): From Island to Island-chain Formation and Co Intercalation. *Surf. Sci.* **2002**, *511*, 379−386.
(36) Ataca, C.; Sahin, H.; Ciraci, S. Stable, Single-Layer MX_2 Transition-Metal Oxides and Dichalcogenides in a Honeycomb-Like Structure. *J. Phys. Chem. C* **2012**, *116*, 8983−8999.
(37) Gong, C.; Huang, C.; Miller, J.; Cheng, L.; Hao, Y.; Cobden, D.; Kim, J.; Ruoff, R. S.; Wallace, R. M.; Cho, K.; Xu, X.; Chabal, Y. J. Metal Contacts on Physical Vapor Deposited Monolayer MoS_2. *ACS Nano* **2013**, *7*, 11350−11357.
(38) Liu, X.; Hupalo, M.; Wang, C.-Z.; Lu, W.-C.; Thiel, P. A.; Ho, K.-M.; Tringides, M. C. Growth Morphology and Thermal Stability of Metal Islands on Graphene. *Phys. Rev. B* **2012**, *86*, 081414.
(39) Li, L.; Wang, Y.; Xie, S.; Li, X.-B.; Wang, Y.-Q.; Wu, R.; Sun, H.; Zhang, S.; Gao, H.-J. Two-Dimensional Transition Metal Honeycomb Realized: Hf on Ir(111). *Nano Lett.* **2013**, *13*, 4671−4674.
(40) White, R. M.; *Quantum Theory of Magnetism*, 3rd, ed; Springer-Verlag: Berlin, 2007.
(41) Prasai, D.; Tuberquia, J. C.; Harl, R. R.; Jennings, G. K.; Bolotin, K. I. Graphene: Corrosion-Inhibiting Coating. *ACS Nano* **2012**, *6*, 1102−1108.
(42) Novoselov, K. S.; Geim, A. K.; Morozov, S. V.; Jiang, D.; Zhang, Y.; Dubonos, S. V.; Grigorieva, I. V.; Firsov, A. A. Electric Field Effect in Atomically Thin Carbon Films. *Science* **2004**, *306*, 666−669.
(43) Nair, R. R.; Wu, H. A.; Jayaram, P. N.; Grigorieva, I. V.; Geim, A. K. Unimpeded Permeation of Water through Helium-Leak-Tight Graphene-Based Membranes. *Science* **2012**, *335*, 442−444.
(44) Surwade, S. P.; Li, Z. T.; Liu, H. T. Thermal Oxidation and Unwrinkling of Chemical Vapor Deposition-Grown Graphene. *J. Phys. Chem. C* **2012**, *116*, 20600−20606.
(45) Ma, Y.; Dai, Y.; Guo, M.; Niu, C.; Huang, B. Graphene Adhesion on MoS_2 Monolayer: An *ab initio* Study. *Nanoscale* **2011**, *3*, 3883−3887.
(46) Cao, C.; Wu, M.; Jiang, J. Z.; Cheng, H. P. Transition Metal Adatom and Dimer Adsorbed on Graphene: Induced Magnetization and Electronic Structures. *Phys. Rev. B* **2010**, *81*, 205424.
(47) Zhao, J.; Deng, Q.; Bachmatiuk, A.; Sandeep, G.; Popov, A.; Eckert, J.; Rümmeli, M. H. Free-Standing Single-Atom-Thick Iron Membranes Suspended in Graphene Pores. *Science* **2014**, *343*, 1228−1232.